Using EOF Analysis over a Large Area for Assessing the Climate Impact of Small-Scale Afforestation in a Semiarid Region

G. YOSEF

Department of Applied Mathematics, Israel Institute for Biological Research, Ness Ziona, Israel

P. ALPERT AND C. PRICE

Department of Geosciences, Tel Aviv University, Tel Aviv, Israel

E. ROTENBERG AND D. YAKIR

Department of Earth and Planetary Sciences, Weizmann Institute of Science, Rehovot, Israel

(Manuscript received 17 July 2016, in final form 12 June 2017)

ABSTRACT

The authors suggest an approach to analyze the effects of small-scale afforestation on the surrounding climate of a large heterogenic area. While simple statistics have difficulty identifying the effect, here a well-known eigenvector technique is used to overcome several specific challenges that result from a limited research region, complex topography, and multiple atmospheric circulation patterns. This approach is applied to investigate the influence of the isolated Yatir forest, at the north edge of Israel's Negev Desert. It was found that this forest does influence the daily climate, primarily seen in the main pattern of the empirical orthogonal function (EOF) of temperature and humidity. The EOF explains 93% and 80%, respectively, of the total variance in the data. Although the Yatir forest is small, it is significant in regulating the climate in the nearby surroundings, as it is located in a sharp transition area toward an arid climate. The results are presented as maps of correlation and regression between the normalized principal component time series of each pattern as well as other time series of the raw data and spatially interpolated data stations. Analysis of short-term campaign measurements around the Yatir forest supports the EOF results, and shows the forest's influence to the south, mainly during nighttime when the forest becomes cooler than its surroundings. Overall, results suggest that in areas of transition to semiarid climates, forests regulate the surrounding surface air temperature and humidity fields. Wind analysis based on a complex EOF technique reveals the pattern of the daily cycle of surface wind over the region.

1. Introduction

There is much interest in the impact of land-use change (LUC) on local climate (Costa and Pires 2010; Fall et al. 2010a,b; Brovkin et al. 2013; Deng et al. 2013). Numerical simulations using complex models of the atmosphere have shown that the presence or absence of vegetation could influence the local climate of the region in question, for example, Charney (1975) and Shukla and Mintz (1982). Deforestation and overgrazing, as studied in the Amazon forest and the Sahel zone, decrease precipitation and daytime evapotranspiration and increase average daytime temperature, all because of decreased humidity near the ground and changes in the energy balance; for example, see Otterman (1974), Charney (1975), Idso (1980), Shukla et al. (1990), and Xue and Shukla (1993, 1996). On the other hand, afforestation processes, studied in arid areas like the Sahel, modify the energy balance and accelerate changes of circulation, leading to increased precipitation (Ortiz et al. 2000; Patricola and Cook 2007; Davin et al. 2007; Bonan 2008; Cowling et al. 2009). Studies in central/south Israel on the influence of LUC on climate have found a decrease of the daytime temperature amplitude (Alpert and Mandel 1986), enhancement of convective rainfall due to increased

Supplemental information related to this paper is available at the Journals Online website: https://doi.org/10.1175/JAMC-D-16-0253.s1.

Corresponding author: Dr. Gil Yosef, gily@iibr.gov.il

DOI: 10.1175/JAMC-D-16-0253.1

air humidity, and the creation of thermals that enhance convection (Otterman et al. 1990; Ben-Gai et al. 1993).

Previous studies on the climate impact of LUC over semiarid areas suggest a tight coupling between the atmosphere and land surface (Koster et al. 2004). This coupling is characterized by exceedingly complex nonlinear interactions with extensive degrees of freedom (modes). Consequently, a challenging task in climate science is to find ways to reduce the dimensions of the system and reveal the most important patterns behind the variations (Thompson and Wallace 1998). Numerical climate models (Grotch and MacCracken 1991; IPCC 2007; Maraun et al. 2010) are widely used for analyzing small areas. However, this technique is ineffective for revealing high-resolution or finescale spatial resolution of effects (Lluch-Cota et al. 2003). In addition, the heterogenic distribution of meteorological stations in such areas makes the analysis more complex. To reveal the patterns over small research areas, eigentechniques can be applied to capture most of the variance in the data in a small number of modes (Venegas et al. 1997; Venegas 2001). Each of the modes is represented by its spatial pattern and time series, which are derived from the eigenvalues and eigenvectors of the covariance matrix. Using the efficiency of the eigentechniques, we investigated the impacts of LUC in Israel, caused by changes in land use in the central-north Negev (Otterman et al. 1990; Ben-Gai et al. 1993; Sharon and Angert 1998). This study focused on the Yatir afforestation project (Rotenberg and Yakir 2010). Based on lidar and ceilometers measurements at Yatir, Eder et al. (2015) showed that there is a secondary air circulation created over the forest that likely changes surface air temperature and relative humidity values over the forest relative to the surroundings, thus providing a mechanistic explanation of the connection between the two.

Based on studies mentioned above, we hypothesized that a relatively small-scale afforestation area in a semiarid region can influence the climate of the surrounding area and the Yatir forest was chosen as a case study. We evaluate the forest's contribution to mesometeorological cycles and the scope of the impact of the forest on the local climate. The research was performed on the basis of data collected in the summer months, when there is a semipermanent synoptic circulation pattern that can be isolated, thus enabling us to study the pattern generated by the forest itself. We used simple statistics on the stations' measurements in the area, and showed the difficulty in identifying clearly the influence of the dense vegetation, in particular the small-scale Yatir forest on large research area (see Fig. 2, described in more detail below). Therefore, we used the statistical analysis of eigentechniques in the following procedure: first, using several interpolations on a synthetic database and interpolation schemes; second, directly on the raw data stations, producing interpolated correlation and regression maps (see discussion in the method section).

Eigentechniques were applied to temperature, humidity, and wind observations on a small scale with high temporal (1 h) and spatial (~2.5 km) resolution. Section 2 outlines the method that describes the summer climatology, dataset collection, and generation of synthetic maps by several interpolation methods and briefly introduces the applied methods of eigentechniques. Spatial and temporal patterns of temperature and humidity are presented in section 3. Section 4 summarizes the conclusions.

2. Method

During the summer months, Israel is influenced by two global synoptic circulation patterns: the subtropical high that causes regional subsidence over the eastern Mediterranean with the associated marine inversion (Alpert et al. 1990), and the Persian trough that influences the region through dominance of the northwest winds (Yair and Ziv 1994). Subsidence of the subtropical air creates a stable atmosphere, leading to the creation of thermal circulations, such as the nighttime land breeze and daytime sea breeze along the Mediterranean coast, investigated by Doron and Neumann (1977), Segal et al. (1985), Lieman and Alpert (1993), and Alpert and Rabinovich-Hadar (2003). An additional circulation develops between the coast and the inland mountains as a result of the topographic gradient (Fig. 1a): Anabatic winds are created during the day and enhance the sea breeze. At night a katabatic westward wind strengthens the land breeze. Another dominating circulation is the Red Sea trough that generally creates eastern winds whose strength is modified by the land and sea breezes.

The research area is a region considerably larger than the Yatir forest and was chosen to emphasize the ability of the technique to identify the effects of a small forest on its surroundings. This region includes various geographical features, such as mountain slopes, the coastal plain area, and varying land use (Fig. 1b) and several patches of forest (indicated by the ellipses in Fig. 1a). A larger forest is in the north, along the hills toward Jerusalem, and the smaller Yatir forest is in the south, at the edge of a rapid transition zone from semiarid to arid desert. The black box in Fig. 1a shows the research area between longitude 34.6°E and 35.22°E and between latitude 31.25°N and 31.85°N. The research area is ~3920 km^2.

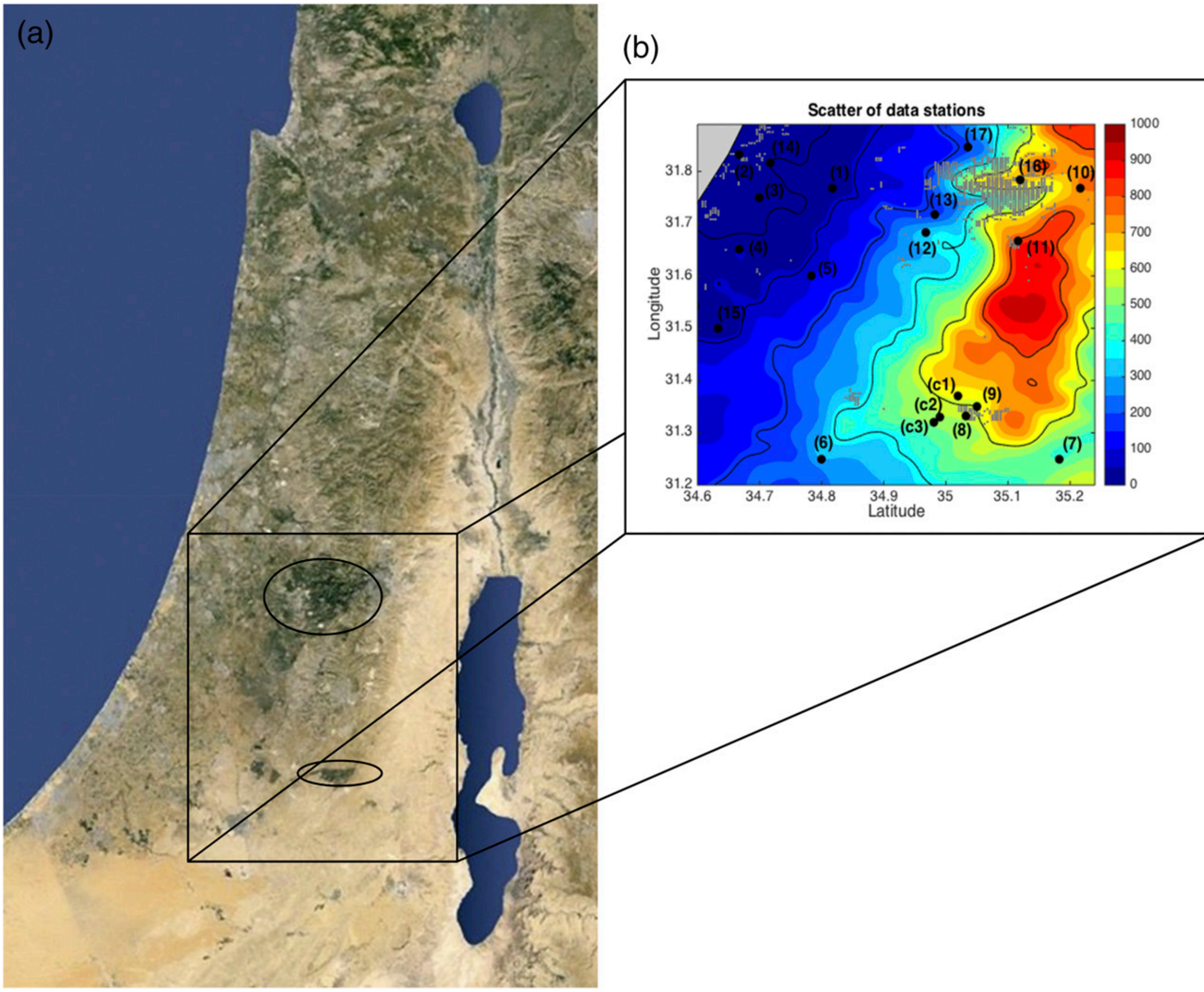

FIG. 1. (a) The box represents the research area in southern Israel, and the black ellipses indicate two main patches of forest in the area. (b) Topography height in the research area based on a digital elevation model (DEM) database. Black dots indicate meteorological stations. Contours and the color scale represent the topography height (m).

We used meteorological station data provided by the Israel Meteorology Service (IMS) as well as data from the Yatir forest and three sites of campaign measurements around the Yatir forest provided by the Department of Earth and Planetary Sciences at the Weizmann Institute. The Yatir forest data collection is automatic, with half-hour resolution, and is converted to hourly resolution to fit the IMS database. The measured parameters are surface air temperature, relative humidity, and wind at surface level for the months of August–September 2002–05 in all the stations, with an additional two stations in the north located in and out of the forest (numbers 16 and 17) for August–September 2013–16 (Table 1). To support empirical orthogonal function (EOF) analysis results, campaign measurements during summertime around Yatir forest were used. Three sites were used, located northeast (c1), west (c2), and southwest of the forest (c3) (Fig. 1b). Two consecutive weeks of hourly resolution at each site were analyzed: in (c1) August 2015, (c2) June 2012, and (c3) August 2013.

The period August–September was chosen as in this period it is easier to observe and isolate the regional circulation (the subtropical ridge creates a marine inversion, and the Persian trough creates western winds) and the local circulation (sea and land breeze, anabatic and katabatic winds). This enabled us to isolate the daily anomalies due to processes related to land coverage.

Limited meteorological stations and their heterogeneous scattering in complex terrain present difficulties for spatial analysis and for defining the spatial extent of climate data. Therefore, spatial interpolation is utilized for building gridded maps. To provide reliable meteorological fields (surface air temperature, relative humidity, and wind), we

TABLE 1. Location of meteorological stations by lat (°N)/lon (°E) and altitude above mean sea level.

No.	Station	Lat	Lon	Alt (m)
1	Revadim	31.77	34.82	90
2	Ashdod	31.83	34.67	10
3	Azrikam	31.75	34.7	30
4	Negba	31.65	34.67	90
5	Lachish	31.6	34.78	125
6	Beer-Sheva	31.25	34.8	280
7	Arad	31.25	35.18	568
8	Yatir	31.33	35.03	650
9	Shany	31.35	35.05	695
10	Jerusalem	31.77	35.22	815
11	Rosh-Tzurim	31.67	35.12	955
12	Netiv H L H	31.68	34.97	285
13	Bet-Gimal	31.72	34.98	360
14	Yavne	31.82	34.72	50
15	Besor	31.27	34.38	106
16	Tzova	31.78	35.12	730
17	Mevo Horon	31.85	35.02	195
c1	Northeast to YF	31.37	35.02	575
c2	East to YF	31.33	34.99	522
c3	Southeast to YF	31.32	34.98	460

compare two different interpolation approaches. The first technique was the combination of linear with the nearest-neighbor interpolation methods (LNN) where the linear interpolation uses two grid point values to define a value of a grid point in between, while the nearest-neighbor interpolation considers only one grid point, closest to the interpolated point used, because of a lack of data at the domain's edges. The second technique was the kriging interpolation (Kr), an advanced geostatistical procedure based on models that include autocorrelation, which weighs the contribution of the measured point according to statistical relationships; for more details see Oliver and Webster (1990) and Cressie (2015). Comparisons between LNN (Fig. S1 in the online supplementary material) and Kr (Figs. 3a–c and 4a–c, described in more detail below) show, in general, the same spatial patterns for the surface air temperature and relative humidity variables; however, they showed different directions of influence on Yatir forest (see discussion in the results section). We based the analysis on Kr interpolation procedure for 3-km grid spacing.

Simple statistical techniques (e.g., the spatial mean, anomaly, and standard deviation) were applied on the stations' measurements. They show that for surface air temperature, the mountain area is characterized with lower mean (Fig. 2a) and anomaly values (Fig. 2b), while higher values are observed on the coastline and in the west slopes of the mountain. The analysis of the relative humidity (Figs. 2d,e) shows that the coastline was observed with the highest values, while the Yatir forest and eastern slopes of a mountain had the lowest values (for further discussion of physical processes, see the results section). The standard deviation (Fig. 2c) shows the effect of the forest in moderating the daily cycle of surface air temperature but over a larger area, which is not obvious in the observation but is confirmed with the EOF (Fig. 3). The relative humidity (Fig. 2f) does not show any effect. These results emphasize the need for a more complex statistical technique to identify a clear influence of the density vegetation, in particular of the small-scale Yatir forest. In the case of eigentechniques it gives an explanation of the phenomenon, its significance, and a unique time series for the pattern.

a. Overview of EOF and complex EOF (CEOF)

The first technique used was the EOF. The technique is widely applied for the analysis of the spatial and temporal variability of large multidimensional datasets and is commonly used in meteorological studies (Lorenz 1956). It can be used to identify and separate the dominant and the underlying processes and essential parameters that in our case control the surface air temperature and relative humidity patterns. Its main goal is to decompose the parameters of the local climate region, and present a few patterns for each variable. As a result, we hope to show the influence of the forest on the local climate. The following procedure of EOF was performed separately for the surface air temperature and the relative humidity. The popular configuration of the raw data matrix, in atmospheric research, is referred to as S-mode analysis and represents the pattern's location (EOF) and the time series of the patterns called principal component (PC). The matrix has the structure of $M \times N$, where M is the space dimensions and N is the shared sampling dimension. This method was adopted by Björnsson and Venegas (1997) and von Storch and Zwiers (1999). EOF analysis is conducted on datasets where the mean is removed from the measurements; the covariance matrix $\mathbf{F}$ can then be constructed [Eq. (1)] as

$$\mathbf{F} = \frac{1}{N}\mathbf{R}^{\mathrm{T}}\mathbf{R}, \tag{1}$$

where $\mathbf{R}$ is the raw data matrix, $\mathbf{R}^{\mathrm{T}}$ is the transpose matrix, and N is the number of samples. Then, reconstructing the raw data $\mathbf{R}$ [Eq. (2)] with a new time series PC and the eigenvectors (EOF),

$$\mathbf{R}(t,x) = \sum_{\mathrm{allEOFs}} \mathrm{PC}(t)\mathrm{EOF}(x). \tag{2}$$

The decomposed patterns are considered empirical models (EOFs), which are orthogonal to each other in space and in time (Mestas-Nuñez and Enfield 1999).

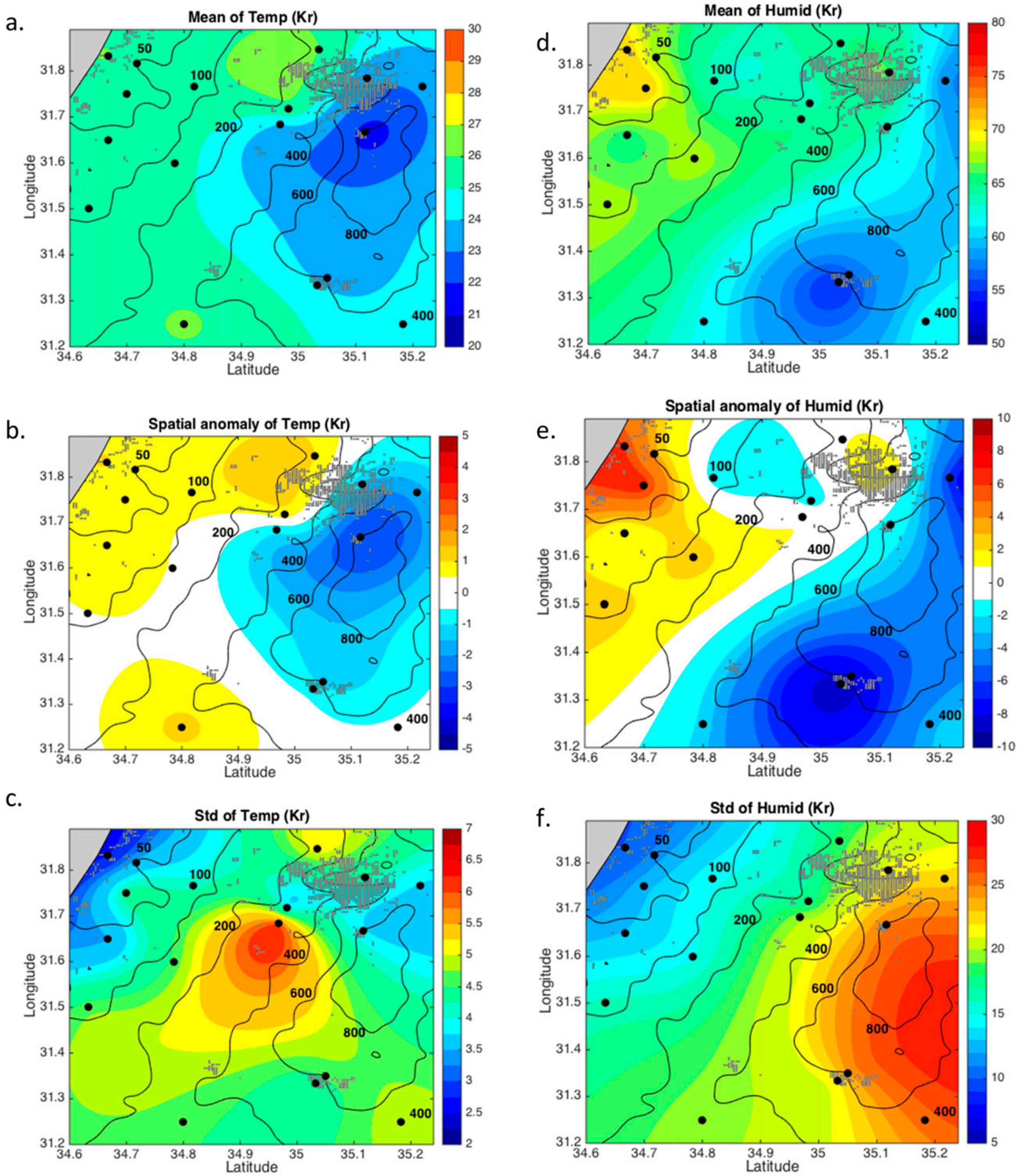

FIG. 2. Spatial interpolation using the Kr method of the meteorological stations (black dots). Surface air temperature (a) mean, (b) spatial anomaly, and (c) spatial standard deviation. The grid maps were prepared with the Kr procedure for 3-km grid spacing. Topography (contours) and vegetation (gray). Contours and color bar units are meters and degrees Celsius, respectively. (d)–(f) As in (a)–(c), but for relative humidity (%).

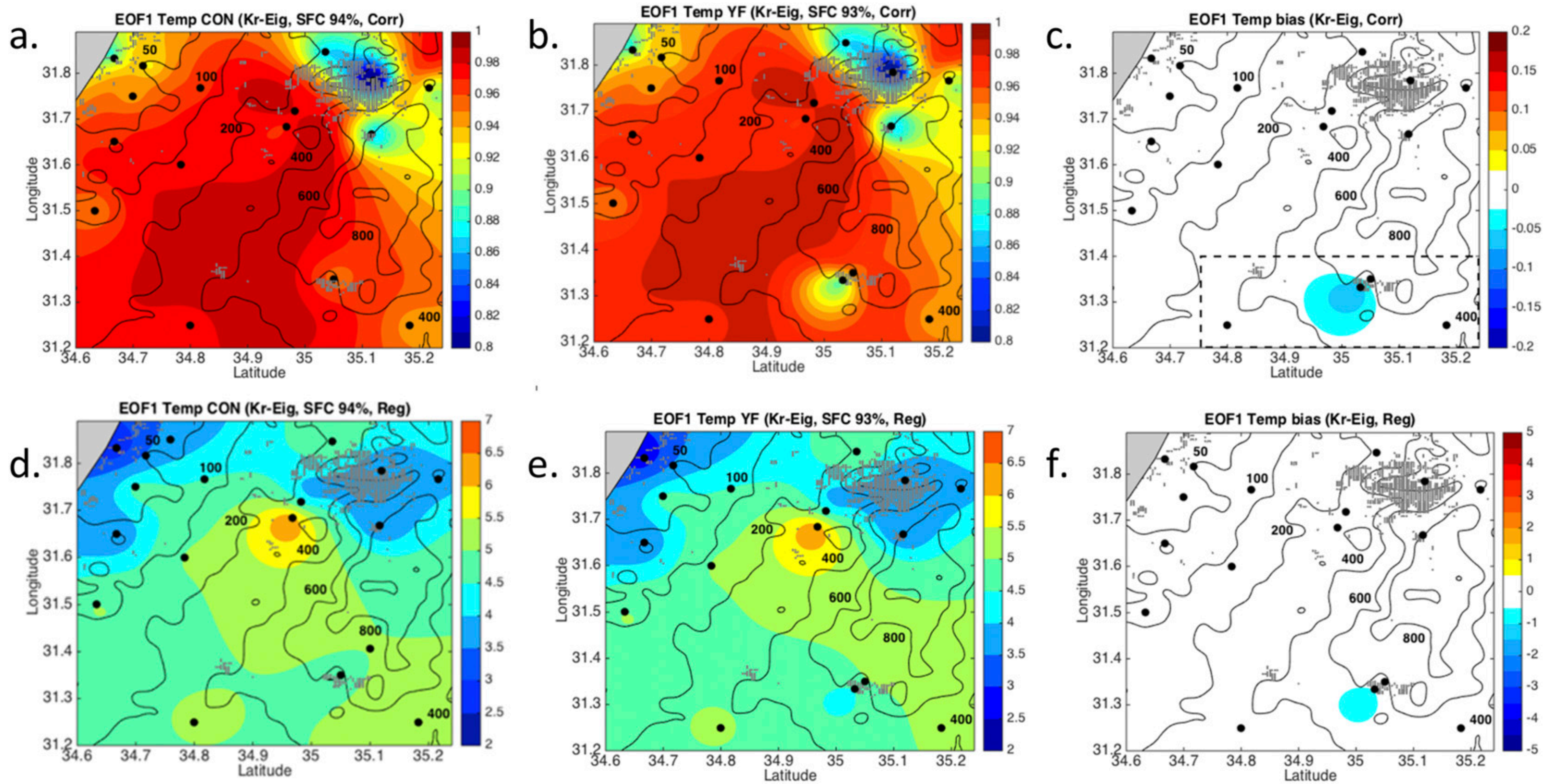

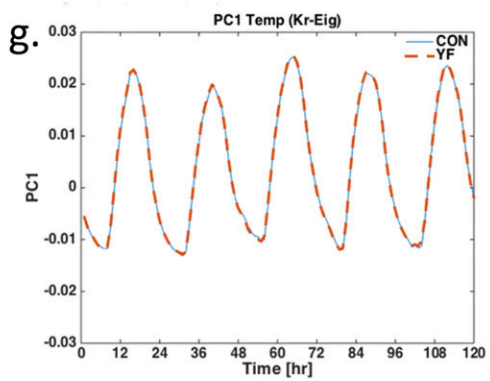

FIG. 3. The first EOF analysis of surface air temperature for the procedure starts with kriging spatial interpolation to the station database and then applying eigentechniques (Kr-Eig). The value at each grid point is the correlation (Corr) and the regression (Reg) coefficient between the time series of the PC and the surface air temperature at that point (with the mean removed; see method section). The interpolation method, fraction of variance explained by the respective modes, and the correlation coefficient are indicated in parentheses in the title of each map. The correlation maps (color shading) show the spatial pattern of (a) CON, (b) YF, and (c) the bias between YF and CON. (d)–(f) As in (a)–(c), but for the regression maps with scale multiplied by 100. (g) The first normalized time series (PC) (the first 5 days are presented) of YF (dashed orange) and CON (solid blue). In the EOF maps, black dots indicate the meteorological stations, contours show topography (m), and vegetation is in gray.

The fraction of each kth mode EOF_k accounts for a variance [Eq. (3)] is

$$\sigma_k = L_k \Big/ \sum_{i=1}^{n} L_i \times 100, \tag{3}$$

where L is the eigenvalue value of the kth eigenvector EOF_k.

The second technique was CEOF, an extension of EOF from a scalar field to vector field, which was used for the wind analysis. Kundu and Allen (1976) introduced this technique with the intention of studying ocean currents (Dominguez and Kumar 2005). The CEOFs procedure is the same as EOF, except from the construction of the covariance matrix $\mathbf{F}_{\text{complex}}$ [Eq. (4)] as

$$\mathbf{F}_{\text{complex}} = \frac{1}{N}\mathbf{RR}^*, \tag{4}$$

where $\mathbf{R}^*$ denotes the complex conjugate transpose, and the $\mathbf{F}_{\text{complex}}$ matrix is Hermitian, which guarantees that the eigenvalues are real.

b. *Output display*

The eigentechnique results were displayed by PCs, which represent normalized time series oscillations of the pattern. To find the location of the pattern in the research region, EOFs are presented as correlation maps resulting from the correlation between the normalized PC time series of each pattern and all other time series of the raw data (stations' or interpolated gridded data). The study area is characterized by high correlation; therefore, the spectrum of the correlation index is limited in order to identify the small biases. In addition, the EOFs are presented as a regression map to investigate the spatial distribution of amplitude of the daily cycle.

We used a sequence of methods: first, kriging interpolation, and second, eigentechniques (Kr-Eig). To verify that there was no "circular reasoning" of the statistical relationship, the eigentechniques were also applied directly on the stations' raw data and then applying kriging interpolation method (Eig-Kr) (Ha et al. 2014; Nazzal et al. 2015).

The MODIS (MCD12Q1) [Land Processes Distributed Active Archive Center (LP DAAC) 2003] land cover was projected to the maps, showing only the relatively dense vegetation class in the research area (woody and closed shrubland).

c. *Analysis procedure*

To show the forest influence, two sets of EOF analyses were done: the first serves as control (CON) and includes all the meteorological stations except the Yatir forest, and the second analysis (YF) includes the Yatir forest station. Then the difference between YF and CON analyses was calculated to show the direct influence of the Yatir forest on the spatial climate and also the fraction of the total variance.

To support the results of the EOFs analysis, the daily average differences map between Yatir forest and the near surrounding meteorological stations was calculated for the surface air temperature and relative humidity (in Figs. 3c and 4c the dashed line represents the analyzed area). Three of the IMS meteorological stations (Arad, Beer-Sheva, and Shany) together with three campaign measurements (c1, c2, and c3) were compared with the Yatir forest station and used to calculate the differences over an hourly time step for two consecutive weeks. Although the measurements were taken in different years, they represent the same summertime season behavior of this region. Also, no synoptic trend was observed between those years. We assume homogeneity over the Yatir forest. Therefore, to calculate the map differences, six points with zero values were used to cover the location of the Yatir forest area according to MODIS's index of relatively dense vegetation (Fig. 8, described in more detail below).

3. Results

a. *Comparisons between LNN and Kr interpolation procedures*

The main biases between the methods are located around the edges of the research area. We expect that the LNN is less accurate along the edges as compared with the Kr method, since it uses the nearest-neighborhood (NN) interpolation, which considers only one grid point as a reference. Another main bias was found in size and direction of the forest influence, measured by the differences between YF and the CON analysis (Figs. S1c,f; Figs. 3c and 4c), which shows a larger area at the Kr interpolation and inconsistent direction of influence with the LNN. The LNN interpolation shows the impact of forest area, which extends northwest of the forest, while Kr interpolation is consistent with observation (Fig. 8, described in more detail below) and shows influence south of the forest.

b. *Temperature analysis*

For the procedure Kr-Eig (Eig-Kr), the main pattern of the surface air temperature field EOF1 at CON and YF analyses account for 94% (86%) and 93% (86%) of the variance, respectively (Figs. 3 and 5). The pattern time series PC1 (Fig. 3g) of CON and YF are intertwined with each other, where the local maxima are obtained at

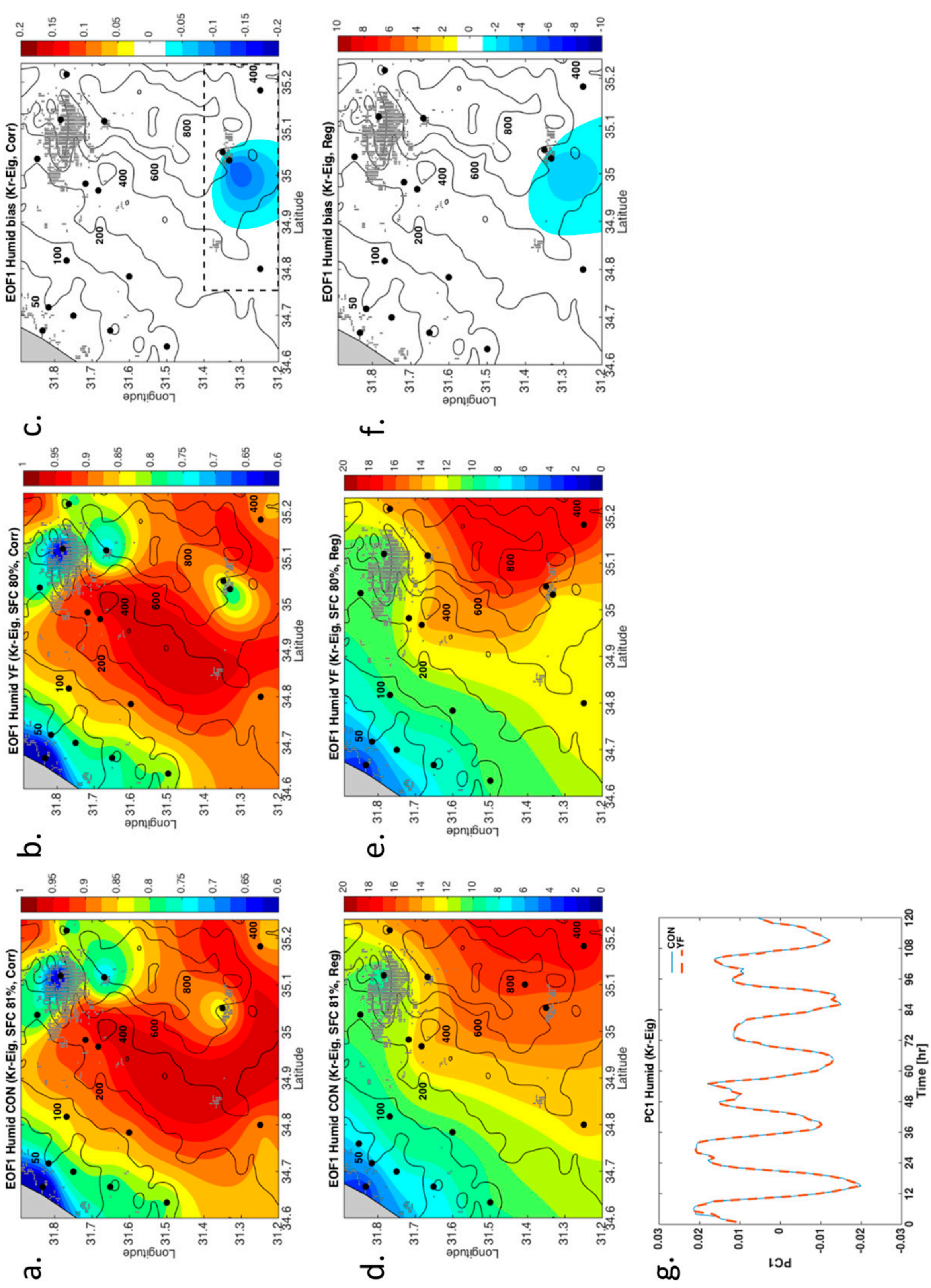

FIG. 4. As in Fig. 3, but for relative humidity analysis.

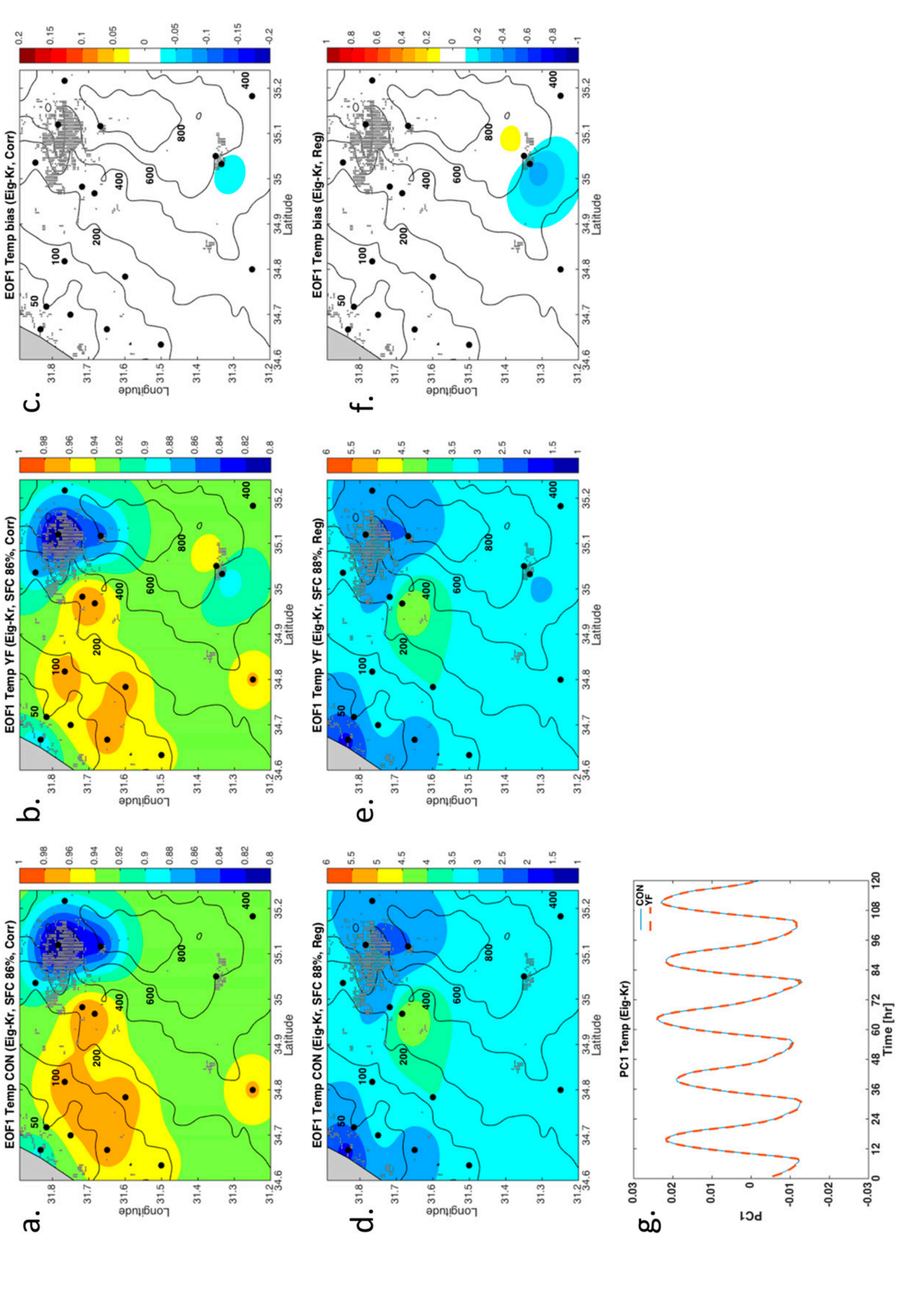

FIG. 5. As in Fig. 3, but for surface air temperature with the procedure starting with applying eigentechniques to the station database and then using kriging for spatial interpolation (Eig-Kr).

around noon and the local minima around midnight. This cycle is a result of the energy balance due to daily solar radiation, with highest intensity every 24 h. The higher-mode EOF3 accounts for 1% (3%) of the variance for the procedure Kr-Eig (Eig-Kr). Although it has a low value, it shows a clear pattern of the forest's influence on the region (Fig. 6).

c. Humidity analysis

For the procedure Kr-Eig, the main pattern of the relative humidity field EOF1 at CON and YF analyses accounts for 81% and 80% of the variance, respectively (Figs. 4a,b). As in the surface air temperature, the pattern time series PC1 (Fig. 4g) of CON and YF are intertwined with each other. The daytime cycle reaches a local maximum peak variance after midnight, until sunrise, when temperatures are lowest, and a local minimum humidity point around noon.

d. Underlying features in the main pattern

For the procedure Kr-Eig, the surface air temperature and relative humidity fields show, in the correlation maps of EOF1 (Figs. 3a,b and 4a,b) for both of the CON and YF analyses, that most of the research area has a high correlation with the PC1, following the 24-h cycle of the daily solar radiation. Within the area of high positive correlation, underlying features at four different locations are revealed: coastline, mountain slopes, mountain, and the forest areas. Where the mountain slope is highest, values are comparable to the other areas. The regression maps show the same features and the same hierarchy of values as the correlation maps, except for the relative humidity variable, which has a maximum over part of the mountain area as compared with the correlation maps that have maximum values in the mountain slopes.

The results shows that the mountain slopes with the height correlation and linear regression values have the highest daily amplitude range of surface air temperature (see stations' comparison in supplemental Fig. S2). The daily amplitude range at the coastline area is affected by the higher humidity, which results in a greenhouse effect and moderates the minimum temperature at night and increases the relative humidity. Around midday, the sea breeze dominates with a northwest wind direction, decreasing the maximum temperature and keeping the highest relative humidity. In the mountain area, clear nights and lower humidity (as a function of distance from the sea) lead to greater upward thermal radiation, which in turn leads to lower minimum surface air temperature and the lowest relative humidity. During the day, the maximum surface air temperature is lowest relative to other areas as a result of the cooling sea breeze (Figs. 7a,b) that flows at a higher altitude, and so it is less affected by the warming surface. In the south, Yatir forest is located in the Negev Desert and is influenced by an arid regional climate, as in Beer Sheva (point 6) and Arad (point 7). However, one should note that in reality, Yatir forest (point 8) is distinct from its surrounding region, with a low correlation and linear regression in relation to its near surroundings.

The third pattern of the surface air temperature (Fig. 6) represents a time series of the dense vegetation areas. EOF3 shows mainly positive correlation and linear regression in the Yatir forest and its surroundings. The factor causing this pattern is vegetation, by moderating between the day and night and therefore regulating the arid climate from its immediate surroundings. Because of its size and its regulating capacity, the clear pattern of the forests appears only in the third pattern, which represents small deviations from the average. The pattern reaches a maximum variance around noon, and a minimum variance during nighttime, which means that the forest creates temperature regulation during the hot hours of the day.

The differences between YF and CON analyses both in surface air temperature and relative humidity show the impact of forest area, which extends southwest of the forest (Figs. 3c,f and 4c,f). The adjacent station Shany (point 9) at the north of the forest determines the north boundary of the forest's influence. The same shape of the forest's influence structure was observed at the daily average differences map, where the forest creates an enclave surrounded with small differences of surface air temperature (Fig. 8b) and relative humidity (Fig. 8d) that stretches south of the forest. There are differences between the two analyses in the forest's influence extending to the southwest in the EOF analysis as compared with the southeast from analyses of difference maps. This can be related to the results of the new campaign sites' measurements west of the forest.

In general, around the enclave to the south, higher temperature and lower relative humidity is observed. Regarding relative humidity, the enclave is smaller and close to the forest size area, meaning the forest's influence is more prominent in surface air temperature than the relative humidity. As the distance from the forest toward the southeast increases, the surface air temperature and relative humidity increase and decrease, respectively. This relates to the transition of climate from semiarid to arid conditions. The shapes of the daily average differences maps are mainly affected by the night hours when surface air temperature around the forest is lower than the surroundings and relative humidity is higher (Figs. 8a,b). The rest of the day is influenced also from the direction and intensity of the wind that acts on the surface air temperature and relative humidity, which limits the forest's influence.

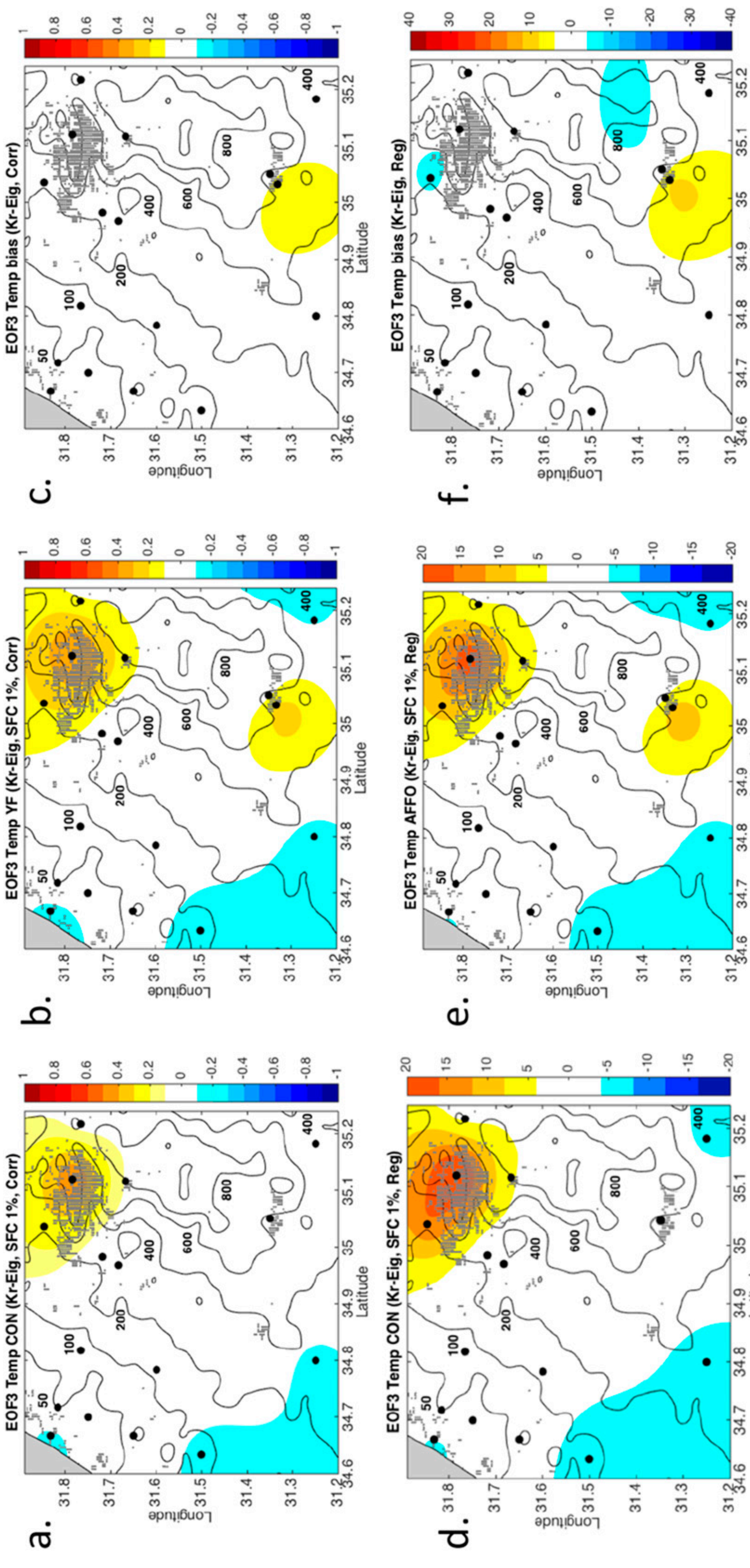

FIG. 6. As in Fig. 3, but for EOF3.

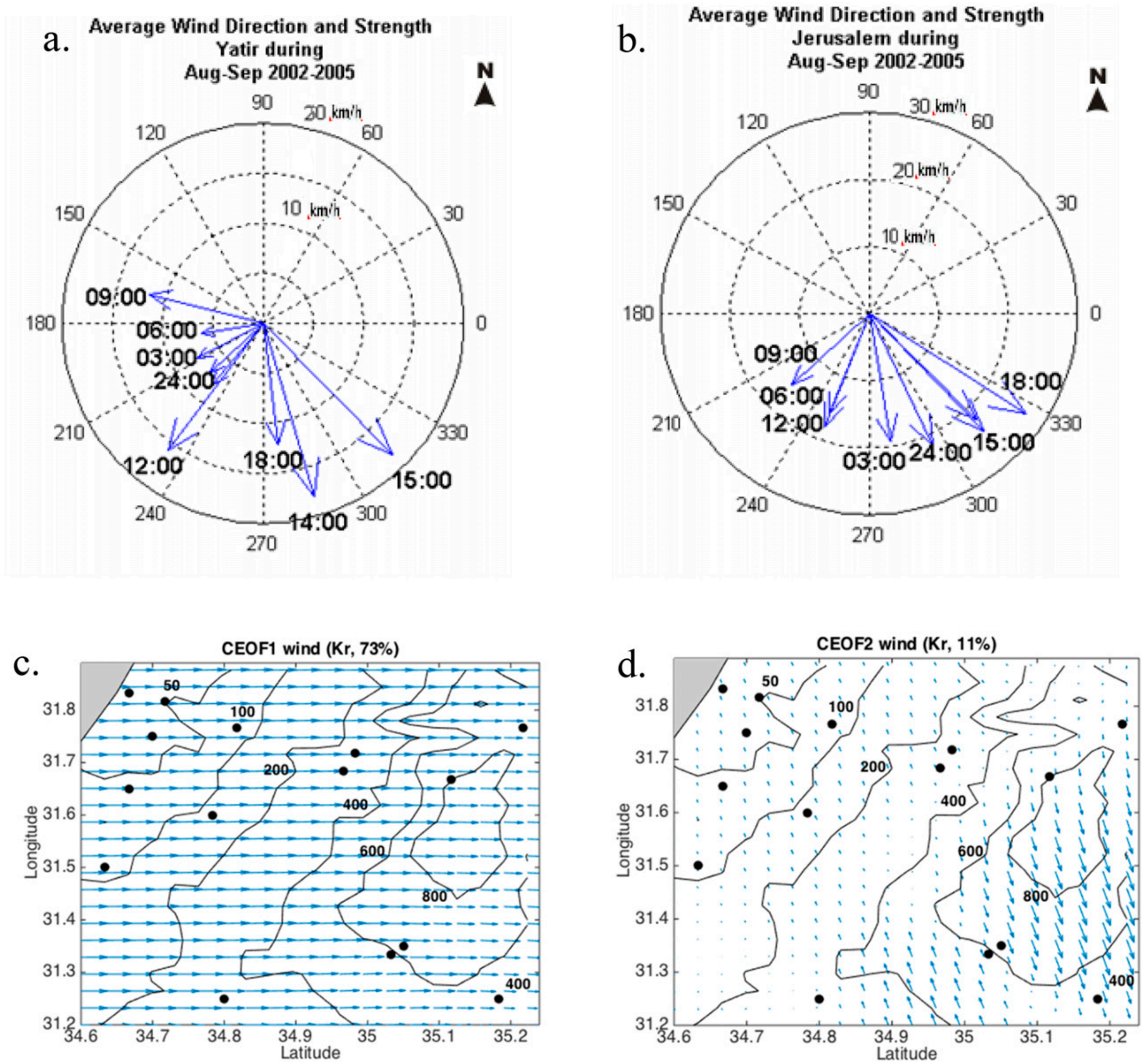

FIG. 7. Wind analysis: hourly average value of wind direction (°) and speed (km h^{-1}) at (a) Yatir and (b) Jerusalem. The main CEOFs analysis of wind: (c) CEOF1 and (d) CEOF2. The value at each grid point is the complex eigenvector. In (c) and (d), black dots indicate the meteorological stations, with topography in contours (m).

Intuitively one would think that the forest's surface air temperature at night should be higher, as the net radiation is higher over the forest than the bare soil, leading to more observed energy. In contrast, Rotenberg and Yakir (2010) presented a study on the radiation budget of a forest in a semiarid area. They show that, in spite of increased radiation absorption due to the forest low albedo and small latent heat flux due to lack of water, such forests develop large sensible heat fluxes, which in turn results in decreasing surface temperature and reduced thermal radiation emission.

For the procedure Eig-Kr the same underlying features (mentioned above) are observed, where the mountain slopes have the highest values in the correlation and regression maps, when compared with the coastline and forest areas (Fig. 5). When compared with the Kr-Eig procedure, Yatir forest is much more prominent in the difference between YF and CON.

e. Wind analysis

The two main patterns of the wind field account for almost 85% of the variance. The first pattern CEOF1 accounts for 73% of the variance and shows the pattern

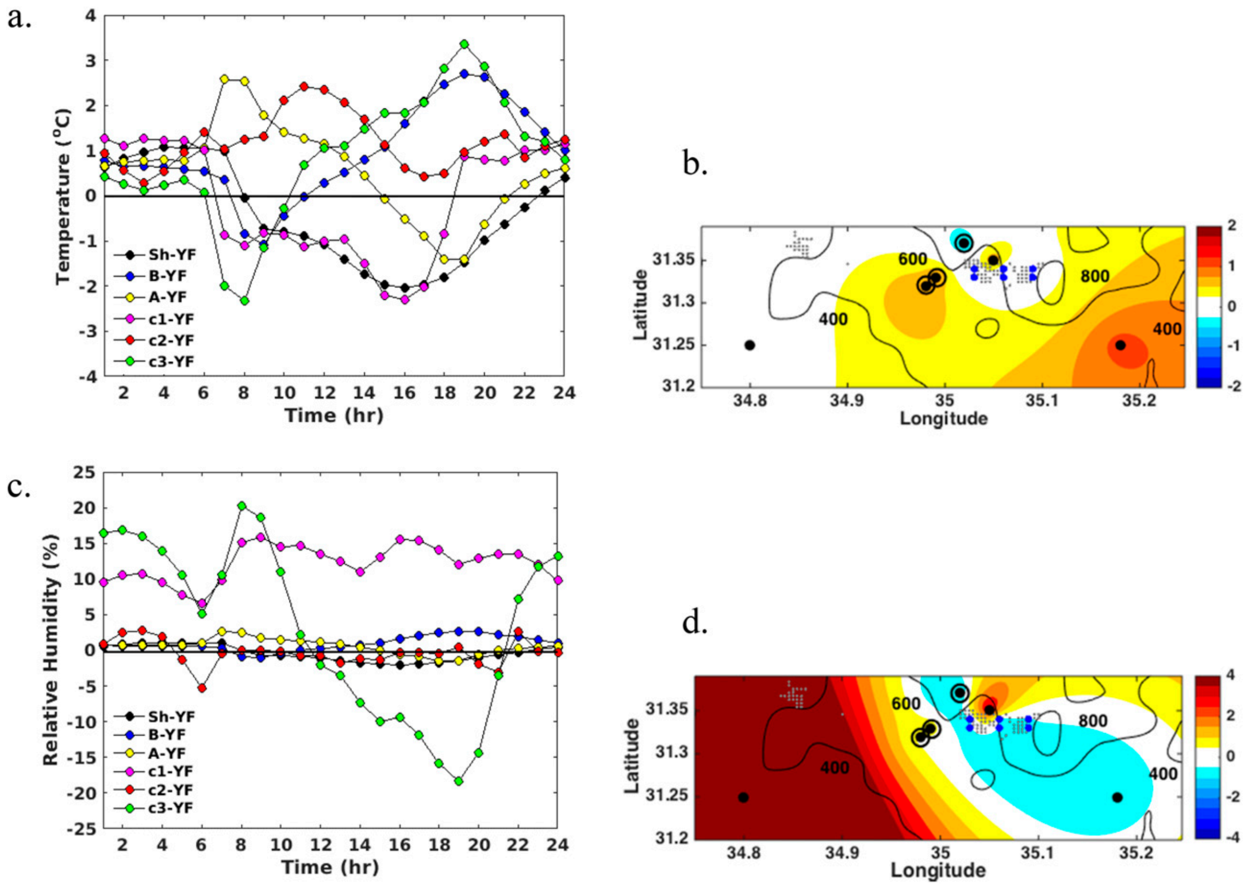

FIG. 8. Daily differences between forest and surroundings: "out" minus "in" of YF for (a),(b) surface air temperature and (c),(d) relative humidity. In (b) and (d), blue dots set with zero values represent the forest location (gray) based on satellite products of MODIS, black dots indicate the IMS meteorological stations, and circled dots represent the campaign measurements (c1, c2, and c3). The grid maps are preformed with the Kr procedure for 3-km grid spacing. Contour (topography) units are in meters, and the color bar represents the difference.

of daily average wind vectors, dominated by the intense western sea breeze. The sea breeze is well developed around noon. Toward evening, it a clearly shows high dominant U wind component (east–west), while the V wind component (north–south) is hardly noticeable (Fig. 7c). The second pattern CEOF2 accounts for 11% of the variance (Fig. 7d) and shows wind directions that are observed after midnight until the early morning. Two distinct areas are shown in CEOF2: the mountain area with a western component and the remaining area including the Yatir forest with weak southeast components, which in the observations appears as easterly winds. The analysis of the results is accompanied by a comparison with those in Segal et al. (1985), which evaluated the wind flows during summer in southern Israel. The results show no influence of the Yatir forest on the creation of horizontal local wind patterns on the scale of the research area. Although we concentrate on the climatological summer season and not the daily cycle, it is important to note that the direction and strength of the wind at different times of the day can change the area influenced by the Yatir forest as was discussed in the previous section.

4. Conclusions

This study attempts to find the effect of small-scale dense vegetation such as Yatir forest on the surrounding local climate, in a large area, using a small number of meteorological stations. It was shown that merely using simple statistics makes it hard to identify, from a large heterogenic area, a clear impact of the small-scale dense vegetation. Therefore, there is a need for a more complex statistical procedure, such as the eigentechniques, that can reveal the forest time series pattern and use it to estimate the spatial influence. Regarding the primary EOF patterns of surface air temperature and relative humidity, it is seen that they are all influenced by the diurnal cycle, so that the approximated maximum or minimum values of the temperature patterns are obtained around 1200 and 2400 local time. We found that in cases of different interpolation procedures, LNN and Kr, on long observation periods, the Yatir forest creates considerable differences in the local climate and its surroundings in both temperature and humidity amplitude regulation. For the procedure Kr-Eig, the main pattern EOF1 (YF analysis) of the surface air temperature and relative humidity fields accounts for 93% and 80% of the variance, respectively. The main patterns in both fields show spatially high correlation with PC1, with underlying features at four different locations. Except for the mountain slopes that have the highest correlation, the coastline, mountain, and Yatir forest areas have lower correlations and thus a lower daily amplitude range. The same results were obtained in the analysis of the regression map, which indicates a strong linear relationship of daily amplitude maximum range in the mountain area when compared with coastline and north forest and Yatir in the south.

To verify that there was no ''circular reasoning,'' the procedures Kr-Eig versus Eig-Kr were examined and showed that there was no significant difference between the results, where the same underlying features of the first pattern were highlighted in both correlation and regression maps. Yatir forest is prominent in the difference between YF and CON using Eig-Kr.

The climate in the region is characterized with a sea breeze during the day that moderates the maximum surface air temperature at the coastline, while in the mountain area it has an important role in reducing the maximum temperature, as it is less affected by the warm surface. At night, surface air temperature at the coastline is moderated by the humidity that acts as a greenhouse effect. In the Yatir forest, the development of large sensible heat fluxes decreases surface air temperature and reduces thermal radiation emission. The location of the forest is in a transition area from semiarid to arid conditions and differentiates itself by its source of moisture. Those effects of lower surface temperature and higher relative humidity become stronger at night when there is no dominant wind, such as the sea breeze, to limit the forest influence.

The analysis of the differences between YF and CON in the two procedures Kr-Eig and Eig-Kr yields the area of the Yatir forest footprint (i.e., the forest's influence), both in surface air temperature and relative humidity. It shows the impact of the forest area that extends southwest of the forest. A similar shape was observed for the daily average differences map based on campaign measurements around the forest, where the forest creates an enclave surrounded with small differences of surface air temperature and relative humidity.

The main pattern of wind field in CEOF1 and CEOF2 accounts for almost 85% of the variance and shows the development of the sea breeze and land breeze, respectively. The Yatir forest does not show an influence on the creation of horizontal local wind patterns on the scale of the research area.

The general conclusion is that the relatively dense vegetation is the basis for a local climate change; for example, 5 km away, in the southern region of the forest center, the day is cooler by 0.5°–1°. The expected dry region afforestation may affect the surroundings. Hence, if the Yatir forest expands, so will its influence, assuming that the climate influence is cumulative. For a higher sensitivity study and in order to quantify the region of influence and extent of the changes, there is a need for a larger number of observations in a more homogeneous regime with further numerical simulations.

Acknowledgments. We thank the Israel Meteorological Service for providing the data of the meteorological stations. The study was partially funded by the German Helmholtz Association within the DESERVE project. We also acknowledge Dr. Yehudah Alexander for fruitful discussions with regard to this work.

REFERENCES

Alpert, P., and M. Mandel, 1986: Wind variability—An indicator for a mesoclimatic change in Israel. *J. Climate Appl. Meteor.*, **25**, 1568–1576, doi:10.1175/1520-0450(1986)025<1568:WVIFAM>2.0.CO;2.

——, and M. Rabinovich-Hadar, 2003: Pre- and post-sea-breeze frontal lines—A meso-γ-scale analysis over south Israel. *J. Atmos. Sci.*, **60**, 2994–3008, doi:10.1175/1520-0469(2003)060<2994:PAPFLM>2.0.CO;2.

——, R. Abramsky, and B. U. Neeman, 1990: The prevailing summer synoptic system in Israel—Subtropical high, not Persian Trough. *Isr. J. Earth Sci.*, **39**, 93–102.

Ben-Gai, T., A. Bitan, A. Manes, and P. Alpert, 1993: Long-term change in October rainfall patterns in southern Israel. *Theor. Appl. Climatol.*, **46**, 209–217, doi:10.1007/BF00865708.

Björnsson, H., and S. A. Venegas, 1997: A manual for EOF and SVD analyses of climate data. CCGCR Rep. 97–1, McGill University, 52 pp.

Bonan, G. B., 2008: Forests and climate change: Forcings, feedbacks, and the climate benefits of forests. *Science*, **320**, 1444–1449.

Brovkin, V., L. Boysen, T. Raddatz, V. Gayler, A. Loew, and M. Claussen, 2013: Evaluation of vegetation cover and land-surface albedo in MPI-ESM CMIP5 simulations. *J. Adv. Model. Earth Syst.*, **5**, 48–57, doi:10.1029/2012MS000169.

Charney, J. G., 1975: Dynamics of deserts and drought in the Sahel. *Quart. J. Roy. Meteor. Soc.*, **101**, 193–202, doi:10.1002/qj.49710142802.

Costa, M. H., and G. F. Pires, 2010: Effects of Amazon and central Brazil deforestation scenarios on the duration of the dry season in the arc of deforestation. *Int. J. Climatol.*, **30**, 1970–1979, doi:10.1002/joc.2048.

Cowling, S. A., C. D. Jones, and P. M. Cox, 2009: Greening the terrestrial biosphere: Simulated feedbacks on atmospheric heat and energy circulation. *Climate Dyn.*, **32**, 287–299, doi:10.1007/s00382-008-0481-8.

Cressie, N., 2015: *Statistics for Spatial Data.* John Wiley and Sons, 928 pp.

Davin, E. L., N. de Noblet-Ducoudré, and P. Friedlingstein, 2007: Impact of land cover change on surface climate: Relevance of the radiative forcing concept. *Geophys. Res. Lett.*, **34**, L13702, doi:10.1029/2007GL029678.

Deng, X., C. Zhao, and H. Yan, 2013: Systematic modeling of impacts of land use and land cover changes on regional climate: A review. *Adv. Meteor.*, 317678, doi:10.1155/2013/317678.

Dominguez, F., and P. Kumar, 2005: Dominant modes of moisture flux anomalies over North America. *J. Hydrometeor.*, **6**, 194–206, doi:10.1175/JHM417.1.

Doron, E., and J. Neumann, 1977: Land and mountain breezes with special attention to Israel's Mediterranean coastal plain. *Isr. Meteor. Res. Pap.*, **1**, 109–122.

Eder, F., F. De Roo, E. Rotenberg, D. Yakir, H. P. Schmid, and M. Mauder, 2015: Secondary circulations at a solitary forest surrounded by semi-arid shrubland and their impact on eddy-covariance measurements. *Agric. For. Meteor.*, **211**, 115–127, doi:10.1016/j.agrformet.2015.06.001.

Fall, S., D. Niyogi, A. Gluhovsky, R. A. Pielke, E. Kalnay, and G. Rochon, 2010a: Impacts of land use land cover on temperature trends over the continental United States: Assessment using the North American Regional Reanalysis. *Int. J. Climatol.*, **30**, 1980–1993, doi:10.1002/joc.1996.

——, N. S. Diffenbaugh, D. Niyogi, R. A. Pielke, and G. Rochon, 2010b: Temperature and equivalent temperature over the United States (1979–2005). *Int. J. Climatol.*, **30**, 2045–2054, doi:10.1002/joc.2094.

Grotch, S. L., and M. C. MacCracken, 1991: The use of general circulation models to predict regional climatic change. *J. Climate*, **4**, 286–303, doi:10.1175/1520-0442(1991)004<0286:TUOGCM>2.0.CO;2.

Ha, H., J. R. Olson, L. Bian, and P. A. Rogerson, 2014: Analysis of heavy metal sources in soil using kriging interpolation on principal components. *Environ. Sci. Technol.*, **48**, 4999–5007, doi:10.1021/es405083f.

Idso, S. B., 1980: Surface energy balance and genesis of deserts. *Arch. Meteor. Geophys. Bioklimatol.*, **30A**, 253–260.

IPCC, 2007: *Climate Change 2007: The Physical Science Basis*. Cambridge University Press, 996 pp.

Koster, R. D., and Coauthors, 2004: Regions of strong coupling between soil moisture and precipitation. *Science*, **305**, 1138–1140, doi:10.1126/science.1100217.

Kundu, P. K., and J. S. Allen, 1976: Some three-dimensional characteristics of low-frequency current fluctuations near the Oregon coast. *J. Phys. Oceanogr.*, **6**, 181–199, doi:10.1175/1520-0485(1976)006<0181:STDCOL>2.0.CO;2.

Land Processes Distributed Active Archive Center (LP DAAC), 2003: Land cover type yearly L3 Global 0.05Deg CMG MCD12C1. USGS Earth Resources Observation and Science (EROS) Center, Sioux Falls, South Dakota, accessed 1 January 2012, https://lpdaac.usgs.gov.

Lieman, R., and P. Alpert, 1993: Investigation of the planetary boundary layer height variations over complex terrain. *Bound.-Layer Meteor.*, **62**, 129–142, doi:10.1007/BF00705550.

Lluch-Cota, D. B., W. S. Wooster, S. R. Hare, D. Lluch-Belda, and A. Parés-Sierra, 2003: Principal modes and related frequencies of sea surface temperature variability in the Pacific coast of North America. *J. Oceanogr.*, **59**, 477–488, doi:10.1023/A:1025592616562.

Lorenz, E. N., 1956: Empirical orthogonal functions and statistical weather prediction. Department of Meteorology, Massachusetts Institute of Technology, 49 pp.

Maraun, D., and Coauthors, 2010: Precipitation downscaling under climate change: Recent developments to bridge the gap between dynamical models and the end user. *Rev. Geophys.*, **48**, RG3003, doi:10.1029/2009RG000314.

Mestas-Nuñez, A. M., and D. B. Enfield, 1999: Rotated global modes of non-ENSO sea surface temperature variability. *J. Climate*, **12**, 2734–2746, doi:10.1175/1520-0442(1999)012<2734:RGMONE>2.0.CO;2.

Nazzal, Y., F. K. Zaidi, I. Ahmed, H. Ghrefat, M. Naeem, N. S. Al-Arifi, S. A. Al-Shaltoni, and K. M. Al-Kahtany, 2015: The combination of principal component analysis and geostatistics as a technique in assessment of groundwater hydrochemistry in arid environment. *Curr. Sci.*, **108**, 1138–1145.

Oliver, M. A., and R. Webster, 1990: Kriging: A method of interpolation for geographical information systems. *Int. J. Geogr. Inf. Syst.*, **4**, 313–332, doi:10.1080/02693799008941549.

Ortiz, J., T. Guilderson, J. Adkins, M. Sarnthein, L. Baker, and M. Yarusinsky, 2000: Abrupt onset and termination of the African Humid Period: Rapid climate responses to gradual insolation forcing. *Quat. Sci. Rev.*, **19**, 347–361, doi:10.1016/S0277-3791(99)00081-5.

Otterman, J., 1974: Baring high-albedo soils by overgrazing: A hypothesized desertification mechanism. *Science*, **186**, 531–533, doi:10.1126/science.186.4163.531.

——, A. Manes, S. Rubin, P. Alpert, and D. C. Starr, 1990: An increase of early rains in southern Israel following land-use change? *Bound.-Layer Meteor.*, **53**, 333–351, doi:10.1007/BF02186093.

Patricola, C. M., and K. H. Cook, 2007: Dynamics of the West African monsoon under mid-Holocene precessional forcing: Regional climate model simulations. *J. Climate*, **20**, 694–716, doi:10.1175/JCLI4013.1.

Rotenberg, E., and D. Yakir, 2010: Contribution of semi-arid forests to the climate system. *Science*, **327**, 451–454, doi:10.1126/science.1179998.

Segal, M., Y. Mahrer, R. A. Pielke, and R. C. Kessler, 1985: Model evaluation of the summer daytime induced flows over southern Israel. *Isr. J. Earth Sci.*, **34**, 39–46.

Sharon, D., and A. Angert, 1998: Long-term changes in northern Negev rains from a regional perspective (in Hebrew). *Meteor. Isr.*, **5**, 38–50.

Shukla, J., and Y. Mintz, 1982: Influence of land-surface evapotranspiration on the earth's climate. *Science*, **215**, 1498–1501, doi:10.1126/science.215.4539.1498.

——, C. Nobre, and P. Sellers, 1990: Amazon deforestation and climate change. *Science*, **247**, 1322–1325, doi:10.1126/science.247.4948.1322.

Thompson, D. W., and J. M. Wallace, 1998: The Arctic Oscillation signature in the wintertime geopotential height and temperature fields. *Geophys. Res. Lett.*, **25**, 1297–1300, doi:10.1029/98GL00950.

Venegas, S. A., 2001: Statistical methods for signal detection in climate. Danish Center for Earth System Science Rep. 2, 96 pp.

——, L. A. Mysak, and D. N. Straub, 1997: Atmosphere–ocean coupled variability in the South Atlantic. *J. Climate*, **10**, 2904–2920, doi:10.1175/1520-0442(1997)010<2904:AOCVIT>2.0.CO;2.

Von Storch, H., and F. W. Zwiers, 1999: *Statistical Analysis in Climate Research.* Cambridge University Press, 499 pp.

Xue, Y., and J. Shukla, 1993: The influence of land surface properties on Sahel climate. Part I: Desertification. *J. Climate*, **6**, 2232–2245, doi:10.1175/1520-0442(1993)006<2232:TIOLSP>2.0.CO;2.

——, and ——, 1996: The influence of land surface properties on Sahel climate. Part II: Afforestation. *J. Climate*, **9**, 3260–3275, doi:10.1175/1520-0442(1996)009<3260:TIOLSP>2.0.CO;2.

Yair, Y., and B. Ziv, 1994: *An Introduction to Meteorology.* Open University Press, 411 pp.